Journal of Zhejiang University-SCIENCE A (Applied Physics & Engineering)
ISSN 1673-565X (Print); ISSN 1862-1775 (Online)
www.jzus.zju.edu.cn; www.springerlink.com
E-mail: jzus@zju.edu.cn

Mechanical, acoustical, and optical properties of several Li-Si alloys: a first-principles study*#

Xiao-hong LI†[1,2], Hong-ling CUI[1], Rui-zhou ZHANG[1]

[1]*College of Physics and Engineering, Henan University of Science and Technology, Luoyang 471023, China*

[2]*Henan Key Laboratory of Photoelectric Energy Storage Materials and Applications, Luoyang 471023, China*

†E-mail: lorna639@yeah.net

Received Feb. 15, 2019; Revision accepted July 21, 2019; Crosschecked July 25, 2019

Abstract: Owing to their excellent theoretical capacity, Li-Si alloys have been extensively investigated as potential Lithium-ion batteries. Knowledge of the mechanical, acoustical, and optical properties of Li-Si alloys is important in order to improve battery performance. In the present study, we calculated the mechanical, acoustical, and optical properties of several Li-Si alloys theoretically. Our investigation confirms the mechanical stability of these Li-Si alloys. With increasing lithium content, Li-Si alloys become increasingly vulnerable to shape deformation as the number of Si-Si bonds decreases. The analysis of elastic moduli shows that the bulk modulus increases with the increase of lithium contents. $Li_{22}Si_5$ has the strongest anisotropic Young's modulus. The sequence of degree of anisotropic Young's modulus is $Li_{22}Si_5$>$Li_{15}Si_4$>LiSi>$Li_{17}Si_4$>$Li_{12}Si_7$>$Li_{13}Si_4$. From an analysis of the anisotropy of acoustic velocity, the transverse velocities are shown to be less than the corresponding longitudinal acoustic velocities. The longitudinal wave of the cubic system is the fastest along the [111] direction, while it is the fastest along the [001] direction for the orthorhombic system and the [010] direction for the tetragonal system. In addition, all the studied Li-Si alloys have relatively low thermal conductivities and show a higher anisotropy when photon energies are lower than 20 eV. We conclude that the studied Li-Si alloys are promising dielectric materials.

Key words: Mechanical properties; Thermal conductivity; Lithium-ion batteries; Elastic anisotropy; First-principles calculations
https://doi.org/10.1631/jzus.A1900050 **CLC number:** O469

1 Introduction

Electrical energy can be transformed into chemical energy by lithium-ion batteries (LIBs), and can be transformed back when needed. LIBs have, therefore, been widely used for electric devices and electric vehicles in recent years, and have stimulated an intensive search for new high-capacity electrodes (Wang et al., 2015; Zhao et al., 2016). As a potential anode material, silicon has attracted much attention because of its low working potential and high theoretical specific capacity. The theoretical capacity of silicon is 4200 mAh/g, about 10 times higher than that of graphite (372 mAh/g) (Zhang et al., 2010). But silicon has a large volume expansion (400%) and internal stress (up to 2 GPa) during cycling. This leads to a low cycle ability and limits practical applications (McDowell et al., 2013; Zeilinger et al., 2013). However, silicon can host lithium, and this property is attracting much attention as it makes Li-Si alloys potential candidates for the next-generation of high energy-density anode materials for rechargeable LIBs (Zhao et al., 2011; Tipton et al., 2013; Zheng et al., 2017).

* Project supported by the National Natural Science Foundation of China (No. U1304111) and the Foundation of the Innovation Team of Henan University of Science and Technology (No. 2015XTD001), China
# Electronic supplementary materials: The online version of this article (https://doi.org/10.1631/jzus.A1900050) contains supplementary materials, which are available to authorized users
ORCID: Xiao-hong LI, https://orcid.org/0000-0003-2450-4476

The Li-Si system (Li_xSi_y) is therefore a new potential anode for LIBs (Wu et al., 2012; Su et al., 2014; Min et al., 2016; Sun et al., 2016), and offers higher theoretical capacities, for example 4212 mAh/g for $Li_{22}Si_5$ (Chevrier et al., 2009) and 3579 mAh/g for $Li_{15}Si_4$ (Obrovac and Christensen, 2004; Key et al., 2009). Many experimental and theoretical studies have been performed to investigate the Li-Si system. Chevrier et al. (2010) reported on the charge transfer, electronic structure, and lattice vibrations of the crystalline Li-Si phases, and confirmed their structures. Braga et al. (2014) investigated the optimized Li-Si alloy thermodynamically. Schwalbe et al. (2017) investigated the thermodynamic properties and elastic constants of lithium silicon. Research has shown that the Li-Si alloy suffers capacity fade and does not form a stable solid electrolyte interphase layer (Xu and von Cresce, 2011; Zhang, 2011). In order to solve this problem, it is of importance to explore the mechanical properties of these alloys (Cheng and Verbrugge, 2010; Shenoy et al., 2010).

Mechanical and acoustical properties are important for Li-Si phases to be used in LIBs to improve battery performance. Ratchford et al. (2011, 2012) measured Young's modulus (E) of $Li_{12}Si_7$ and $Li_{22}Si_5$. The measured E is 52.0 GPa for $Li_{12}Si_7$ and 35.4 GPa for $Li_{22}Si_5$. Shenoy et al. (2010) reported the E value of $Li_{22}Si_5$ to be about 78 GPa, twice that measured by Ratchford et al. (2011). Ratchford et al. (2011) thought that the disagreement did not arise from the testing procedure or from microstructural variables in these alloys. It is necessary therefore to theoretically investigate the mechanical and acoustical properties of Li-Si alloys. We cannot find reference to research on the mechanical and acoustical properties of Li-Si alloys (LiSi, $Li_{12}Si_7$, $Li_{13}Si_4$, $Li_{15}Si_4$, $Li_{17}Si_4$, and $Li_{22}Si_5$). Fig. S1 in the electronic supplementary materials presents the crystal structures of these Li-Si alloys.

The lithium contents of LiSi, $Li_{12}Si_7$, $Li_{13}Si_4$, $Li_{15}Si_4$, $Li_{17}Si_4$, and $Li_{22}Si_5$ are 19.8%, 29.8%, 44.5%, 48.1%, 51.2%, and 52.1%, respectively. In this paper, we describe the investigation of the mechanical, acoustical, and optical properties of these Li-Si alloys and explain the effect of lithium concentration on their properties. The fundamental mechanism is elaborated by comparing our results with the available experimental ones.

2 Calculation details

The first-principle calculations were based on CASTEP code (Chen and Yu, 2012) within the density functional theory (DFT). We used the generalized gradient approximation (GGA) of Perdew-Burke-Ernzerhof (PBE) (Perdew et al., 1996) to describe the exchange-correlation interaction, and used ultrasoft pseudo-potential (Furthmüller et al., 2000) to describe the ion-electron interactions. The Broydon-Fletcher-Goldfarb-Shanno (BFGS) method (Pfrommer et al., 1997) was used to optimize these Li-Si alloys. Atomic positions and unit cell shape were fully relaxed. The energy cutoff was 450 eV. The k point mesh in the Monkhorst-Pack scheme was used with 3×3×4 for LiSi, 3×1×2 for $Li_{12}Si_7$, 3×2×6 for $Li_{13}Si_4$, 3×3×3 for $Li_{15}Si_4$, 2×2×2 for $Li_{17}Si_4$, and 2×2×2 for $Li_{22}Si_5$. The self-consistent field (SCF) tolerance of energy and other properties was less than 5×10^{-8} eV and the maximum force tolerance was less than 5×10^{-5} nm.

3 Results and discussion

3.1 Mechanical properties

The elastic constants can be obtained by the stress-strain method (Sin'ko and Smirnov, 2002). LiSi is tetragonal, which should satisfy the mechanical stability criteria mentioned in (Born, 1940). $Li_{12}Si_7$ and $Li_{13}Si_4$ have an orthorhombic structure, with the mechanical stability criteria described by Mouhat and Coudert (2014). $Li_{15}Si_4$, $Li_{17}Si_4$, and $Li_{22}Si_5$ are cubic, and the mechanical stability criteria of the cubic structure are taken from the work of Nye (1985).

Table 1 lists the calculated elastic constants (C_{ij}) of these Li-Si alloys. The elastic constants of these Li-Si alloys satisfy mechanical stability criteria, confirming their mechanical stability. The results calculated by Cui et al. (2012) are also included in Table 1. Overall, our calculated results are generally in agreement with Cui et al. (2012), with some differences, for instance C_{33} for LiSi, C_{11} and C_{22} for $Li_{13}Si_4$. We think that these differences arise from our different calculation method.

It is known that C_{11}, C_{22}, and C_{33} indicate unidirectional compression in the x, y, and z directions, respectively. C_{44}, C_{55}, and C_{66} indicate the resistance

Table 1 Calculated elastic constant C_{ij} (unit: GPa)

Alloy	C_{11}	C_{22}	C_{33}	C_{44}	C_{55}	C_{66}	C_{12}	C_{13}	C_{23}	Reference
LiSi	106	–	83	45	–	38	22	36	–	This study
	101	–	77	45	–	37	19	37	–	Cui et al., 2012
$Li_{12}Si_7$	95	102	103	32	33	27	5	10	10	This study
	92	97	90	28	26	24	5	11	8	Cui et al., 2012
$Li_{13}Si_4$	87	87	87	28	26	33	11	6	4	This study
	74	61	77	23	24	28	17	11	10	Cui et al., 2012
$Li_{15}Si_4$	51	–	–	33	–	–	22	–	–	This study
	52	–	–	30	–	–	28	–	–	Cui et al., 2012
$Li_{17}Si_4$	67	–	–	42	–	–	17	–	–	This study
$Li_{22}Si_5$	50	–	–	38	–	–	22	–	–	This study
	46	–	–	35	–	–	23	–	–	Cui et al., 2012

to shear. C_{12}, C_{23}, and C_{13} indicate the shear components of the elastic constants. For the tetragonal structure of LiSi, C_{11} is higher than C_{33}, which indicates that it is more easily compressible along the z direction than along the x direction (Guechi et al., 2014). C_{66} is smaller than C_{44} for LiSi, indicating that the [100](010) shear is easier than the [100](001) shear (Zeng et al., 2012).

For the orthorhombic structures of $Li_{12}Si_7$ and $Li_{13}Si_4$, C_{11}, C_{22}, and C_{33} are comparable, indicating that there is nearly equal resistance to compression in each of the x, y, and z directions. For $Li_{12}Si_7$, C_{23} is larger than C_{12}, which indicates that this alloy has stronger resistance shear along the z direction than that along the x direction when a force along the x direction is applied. For $Li_{13}Si_4$, C_{12} is larger than C_{23}, so there is a weaker resistance shear along the z direction. The comparable C_{44}, C_{55}, and C_{66} indicate almost the same resistance of shear deformation in the <110>, <100>, and <101> directions.

For the cubic structures of $Li_{15}Si_4$, $Li_{17}Si_4$, and $Li_{22}Si_5$, the larger C_{11} values indicate that these compounds are not easily compressed along the principal axes. However, the mechanical stability of the studied compounds can be influenced because of a smaller C_{12} and C_{44}. For a cubic crystal, ductility relates to the atomic bonding character, which can be represented by the Cauchy pressures (C_{12}-C_{44}) (Mott and Jones, 1958). A positive Cauchy pressure indicates the ductile nature of the materials, while a negative one indicates the brittleness of the material. For $Li_{15}Si_4$, $Li_{17}Si_4$, and $Li_{22}Si_5$, their negative Cauchy pressure indicates the brittleness of these Li-Si alloys.

3.2 Elastic moduli

Elastic moduli such as bulk modulus (B), shear modulus (G), Young's modulus (E), and Poisson's ratio (ν) can be obtained from the Voigt-Reuss-Hill (VRH) approximations (Voigt, 1928; Reuss, 1929; Hill, 1952) and can be determined through individual elastic constants (C_{ij}) (Ravindran et al., 1998). For a tetragonal structure, the equations for calculating the Voigt and Reuss elastic moduli are in (Ravindran et al., 1998). The Voigt and Reuss elastic moduli can be obtained by using the equations in (Reuss, 1929; Anderson, 1963) and (Ravindran et al., 1998) for cubic and orthorhombic structures, respectively. These equations are all listed in Data S1 of the electronic supplementary materials.

The elastic moduli of crystals can be estimated by the arithmetic mean for B and G (Ravindran et al., 1998), E and ν can be obtained through B and G:

$$E=\frac{9BG}{3B+G},\quad \nu=\frac{3B-2G}{2(3B+G)}. \tag{1}$$

The calculated B, G, E, and ν are listed in Table 2. For a comparison, the experimental values (Chevrier et al., 2009; Kim et al., 2011; Ratchford et al., 2012) and the calculated Young's modulus of $Li_{22}Si_5$ by Shenoy et al. (2010) are also included. The predicted result (~78 GPa) (Shenoy et al., 2010) is larger than our calculational one (~60 GPa), and much larger than the experimental one. We conclude that the DFT method overestimates the Young's modulus of $Li_{22}Si_5$. It is the same for $Li_{12}Si_7$ and $Li_{15}Si_4$.

Table 2 Calculated bulk modulus *B*, Young's modulus *E*, shear modulus *G*, Poisson's ratio, and ratio *B*/*G*

Alloy	B_V (GPa)	B_R (GPa)	G_V (GPa)	G_R (GPa)	B (GPa)	G (GPa)	E (GPa)	E_{min} (GPa)	E_{max} (GPa)	ν	B/G	H_v (GPa)
LiSi	53.67	53.55	39.00	37.13	53.61	38.07	92.34	63.86	102.93	0.21	1.41	8.3
$Li_{12}Si_7$	38.89	36.46	36.73	35.81	37.68	36.27	82.38(52[a], 60[b], 52[c])	70.44	101.08	0.14	1.04	12.6
$Li_{13}Si_4$	33.67	33.75	33.40	32.65	33.71	33.03	74.69	66.66	87.04	0.13	1.02	12.1
$Li_{15}Si_4$	31.67	31.67	25.60	21.85	31.67 (28.6[e])	23.72	56.95(37.95)	37.95	64.54	0.20	1.33	6.1
$Li_{17}Si_4$	33.67	33.67	35.20	33.02	33.67	34.11	76.49	59.72	89.60	0.12	0.99	13.0
$Li_{22}Si_5$	31.33	31.33	28.40	22.54	31.33	25.47	60.12 (38[a], 42[b], 35[c], 78[d])	36.35	81.21	0.18	1.23	7.4

[a] Kim et al., 2011; [b] Chevrier et al., 2009; [c] Ratchford et al., 2012; [d] Shenoy et al., 2010; [e] Zeng et al., 2013. B_V: Voigt bulk modulus; B_R: Reuss bulk modulus; G_V: Voigt shear modulus; G_R: Reuss shear modulus; E_{min}: minimum Young's modulus; E_{max}: maximum Young's modulus; H_v: hardness

It is noted that LiSi, $Li_{12}Si_7$, $Li_{13}Si_4$ show larger B and G than $Li_{15}Si_4$, $Li_{17}Si_4$, $Li_{22}Si_5$, which indicates that B decreases with the increasing lithium content and the Li-Si alloys are easier to compress with this increasing content. Thus, LiSi, $Li_{12}Si_7$, and $Li_{13}Si_4$ are less compressible than $Li_{15}Si_4$, $Li_{17}Si_4$, and $Li_{22}Si_5$. In addition, the B values of these Li-Si alloys are larger than their G values except for $Li_{17}Si_4$ because of the smaller number of Si-Si covalent bonds within the increasing lithium content. This implies that these Li-Si alloys are susceptible to shape deformation.

The 3D plot of an isotropic crystal can exhibit a spherical shape, and the degree of anisotropy can be evaluated by the degree of deviation from sphericity (Guechi et al., 2014). Figs. 1 and 2 show the 3D surfaces of B and E, respectively. The directional B and E of the studied materials on other planes are plotted in Fig. S2. The 3D representation of B is spherical for the cubic system, so Fig. 1 only plots the 3D bulk representation of LiSi, $Li_{12}Si_7$, and $Li_{13}Si_4$. Little deviation from sphericity indicates a relatively small elastic anisotropy for LiSi, $Li_{12}Si_7$, and $Li_{13}Si_4$ from the 3D bulk representation. For the 3D Young representation of the studied Li-Si alloys, all the studied Li-Si alloys have significant anisotropy and exhibit butterfly-shaped curves on some planes (Fig. S2).

For $Li_{12}Si_7$, the maximum E is 101.08 GPa along the z direction, and the minimum is 70.44 GPa along the [110] plane. The ratio of the maximum and minimum Young's modulus is 1.43. For $Li_{13}Si_4$, the maximum Young's modulus is 87.04 GPa along the z direction, and the minimum is 66.66 GPa along the [111] plane. The ratio of the maximum and minimum Young's modulus is 1.31. For $Li_{15}Si_4$, $Li_{17}Si_4$, and $Li_{22}Si_5$, the maximum E are 64.54, 89.60, and 81.21 GPa, respectively. The minimum E are 37.95, 59.72, and 36.35 GPa along the <100>, <010>, and <001> directions, respectively. The maximum and minimum E ratios for $Li_{15}Si_4$, $Li_{17}Si_4$, and $Li_{22}Si_5$ are 1.70, 1.50, and 2.23, respectively. The maximum and minimum E ratio for LiSi is 1.61 with a maximum E of 102.93 GPa along the x direction and a minimum E of 63.86 GPa along the z direction. It should be noted that $Li_{22}Si_5$ has the strongest anisotropic Young's modulus and the order of degree of the anisotropic property is $Li_{22}Si_5$>$Li_{15}Si_4$>LiSi>$Li_{17}Si_4$>$Li_{12}Si_7$>$Li_{13}Si_4$. E along the three principal directions can be obtained by (Sun et al., 2013)

$$E_{[100]}=\frac{1}{s_{11}},\quad E_{[010]}=\frac{1}{s_{22}},\quad E_{[001]}=\frac{1}{s_{33}}, \tag{2}$$

and in the $[1\,\bar{1}0]$ and [111] directions,

$$E_{[1\bar{1}0]}=\frac{4}{s_{11}+s_{12}+s_{22}+s_{66}},$$
$$E_{[111]}=\frac{9}{(s_{11}+s_{22}+s_{33})+2(s_{12}+s_{13}+s_{23})+(s_{44}+s_{55}+s_{66})}, \tag{3}$$

where s_{ij} is the elastic compliance constants listed in Table S1.

Eqs. (2) and (3) can be applied to orthorhombic and cubic systems. For a cubic system, s_{11}=s_{22}=s_{33}, s_{12}=s_{13}=s_{23}, and s_{44}=s_{55}=s_{66}.

For a tetragonal crystal, E can be described as

$$E^{-1}=s_{11}(\alpha^4+\beta^4)+s_{33}\gamma^4+2s_{12}\alpha^2\beta^2+2s_{13}(\beta^2\gamma^2+\alpha^2\gamma^2)+s_{44}(\beta^2\gamma^2+\alpha^2\gamma^2)+s_{66}\alpha^2\beta^2, \tag{4}$$

where α, β, and γ are the direction cosines of the [uvw] direction.

Table 3 lists the calculated Young's modulus in various directions for the studied Li-Si alloys. It is noted that E for these alloys is strongly anisotropic in some directions. For example, the ratio of the Young's modulus between the [111] and [100] directions for $Li_{22}Si_5$ is the largest, which implies that Young's

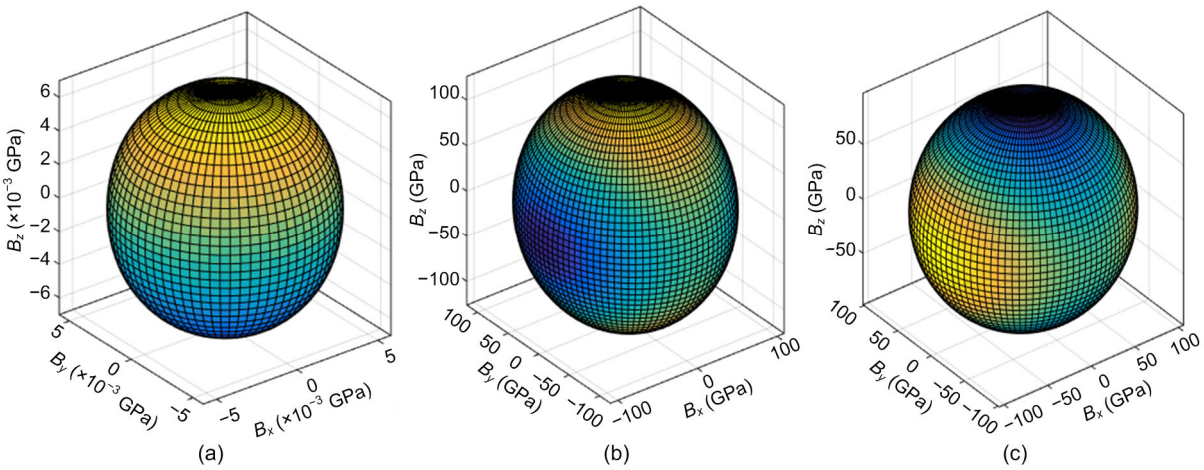

Fig. 1 Three-dimensional dependence of the bulk modulus of LiSi, $Li_{12}Si_7$, and $Li_{13}Si_4$ (B_x, B_y, and B_z are the three components of bulk modulus along x, y, and z axes)

(a) LiSi; (b) $Li_{12}Si_7$; (c) $Li_{13}Si_4$

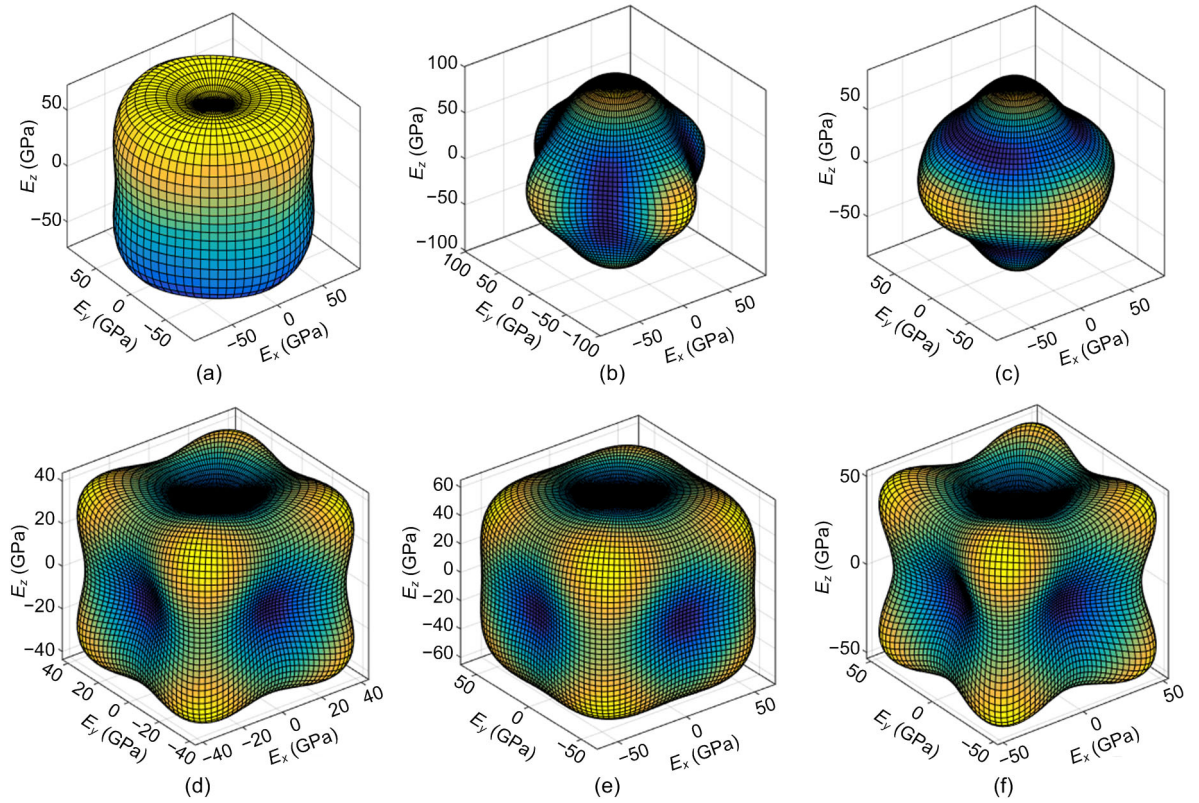

Fig. 2 Three-dimensional dependence of the Young's modulus of the studied Li-Si alloys (E_x, E_y, and E_z are the three components of Young's modulus along the x, y, and z axes)

(a) LiSi; (b) $Li_{12}Si_7$; (c) $Li_{13}Si_4$; (d) $Li_{15}Si_4$; (e) $Li_{17}Si_4$; (f) $Li_{22}Si_5$

modulus of cubic $Li_{22}Si_5$ has the strongest anisotropic property and directional dependence. This result can be further confirmed by the 3D Young representation in Fig. 2. For orthorhombic $Li_{13}Si_4$, the difference in Young's modulus is not so great.

The B/G ratio can measure whether the material is ductile or not (Pugh, 1954). A lower B/G ratio indicates higher brittleness with a critical value of 1.75. A B/G ratio less than 1.75 indicates the brittleness of a compound; a higher ratio shows ductility. B/G values of less than 1.75 for the studied Li-Si alloys confirm their brittle nature in line with the conclusion from the Cauchy pressure.

Poisson's ratio ν is a measure of the compressibility of the material (Savin et al., 1992). ν=0.1 for covalent materials, 0.25 for ionic materials, and 0.33 for metallic materials. From Table 2, ν of $Li_{12}Si_7$, $Li_{13}Si_4$, and $Li_{17}Si_4$ are all close to 0.1, indicating the covalent characteristics of these Li-Si alloys. For LiSi, $Li_{15}Si_4$, and $Li_{22}Si_5$, ν is close to 0.2, indicating ionic contributions are dominant in interatomic bonding. In addition, ν can measure the stability against shear. Smaller Poisson's ratios for $Li_{12}Si_7$, $Li_{13}Si_4$, and $Li_{17}Si_4$ indicate they are relatively stable against shear.

An empirical hardness equation is often used to predict the hardness (H_v) of materials (Chen et al., 2011). Table 2 also lists the calculated hardness of the studied Li-Si alloys. There are no available experimental hardness figures. From Table 2, all the studied Li-Si alloys have a hardness below 20 GPa. $Li_{15}Si_4$ has the lowest.

Table 3 Calculated uniaxial Young's moduli in various directions of the studied Li-Si alloys (unit: GPa)

Alloy	$E_{[100]}$	$E_{[010]}$	$E_{[001]}$	$E_{[1\bar{1}0]}$	$E_{[111]}$
LiSi	102.93	–	63.86	88.17	–
$Li_{12}Si_7$	94.30	100.73	101.08	70.44	72.29
$Li_{13}Si_4$	85.75	85.97	87.04	76.60	67.69
$Li_{15}Si_4$	37.95	37.95	37.95	53.20	58.28
$Li_{17}Si_4$	59.72	59.72	59.72	74.56	78.85
$Li_{22}Si_5$	36.35	36.35	36.35	54.89	62.26

3.3 Elastic anisotropy

Elastic anisotropy is related to the possibility of crack behavior of materials (Guechi et al., 2014) and has been widely used to describe anisotropic behavior in engineering science. Shear anisotropic factors can estimate the degree of anisotropy in the interatomic bonding in different planes.

For an orthorhombic structure, the shear anisotropic factor A_1 denotes the {100} shear planes between the <011> and <010> directions, and is calculated by $A_1=4C_{44}/(C_{11}+C_{33}-2C_{13})$ (Ravindran et al., 1998). A_2 and A_3 are the {010} shear planes between the <101> and <001> directions and the {001} shear planes between the <110> and <010> directions, respectively, and are defined as: $A_2=4C_{55}/(C_{22}+C_{33}-2C_{23})$, and $A_3=4C_{66}/(C_{11}+C_{22}-2C_{12})$. For a cubic system, the elastic anisotropy can be estimated by the Zener ratio A_z: $A_z=2C_{44}/(C_{11}-C_{12})$. For a tetragonal structure, A_1, A_2, and A_3 can be obtained by $A_1=C_{44}(C_{11}+2C_{13}+C_{33})/(C_{11}C_{33}-C_{13}^2)$ for the (010) or (100) plane, $A_2=C_{44}(C_{\mathrm{L}}+2C_{13}+C_{33})/(C_{\mathrm{L}}C_{33}-C_{13}^2)$ for the $(0\bar{1}0)$ plane, $A_3=2C_{66}/(C_{11}-C_{12})$ for the (001) plane, where $C_{\mathrm{L}}=C_{66}+(C_{11}+C_{12})/2$.

For orthorhombic and tetragonal crystals, the factors A_1, A_2, and A_3 equal to one indicate an isotropic crystal, and the deviation from one represents the degree of shear anisotropy of the crystal (Miao et al., 2011). For cubic crystals, the value of zero for A_z indicates the isotropy of materials, other values indicate anisotropy. The anisotropic crystal is the stiffest along the <100> direction if A_z is smaller than one, and the stiffest along the <111> direction if A_z is larger than one (Newnham, 2005). Table 4 lists A_1, A_2, and A_3 of the studied Li-Si alloys. It can be seen that LiSi exhibits a small anisotropy for the (001) plane but has obvious anisotropy for the (010), (100), and $(0\bar{1}0)$ planes. $Li_{12}Si_7$ and $Li_{13}Si_4$ exhibit small anisotropy for all the planes, especially for the (001) plane of $Li_{12}Si_7$ and the $(0\bar{1}0)$ plane of $Li_{13}Si_4$. The A_z values of $Li_{15}Si_4$, $Li_{17}Si_4$, and $Li_{22}Si_5$ are much larger than zero, which indicates that the three compounds are the stiffest along the <111> direction. The percent shear anisotropy A_B and compressibility anisotropy A_G are given as

$$A_{\mathrm{B}}=\frac{B_{\mathrm{V}}-B_{\mathrm{R}}}{B_{\mathrm{V}}+B_{\mathrm{R}}}\times 100\%,\quad A_{\mathrm{G}}=\frac{G_{\mathrm{V}}-G_{\mathrm{R}}}{G_{\mathrm{V}}+G_{\mathrm{R}}}\times 100\%. \tag{5}$$

A_B and A_G equal to zero represent the elastic isotropy, and a value of 100% indicates the largest anisotropy. Table 4 also tabulates A_B and A_G. All the

studied compounds, except for $Li_{12}Si_7$, exhibit small shear anisotropy, but relatively high compressibility anisotropy, especially for $Li_{22}Si_5$ (11%). The universal anisotropic index (A^U) can represent the mechanical anisotropic property (Ranganathan and Ostoja-Starzewski, 2008). A value of zero for A^U indicates an isotropic material. The deviation from zero for A^U indicates the extent of elastic anisotropy. Table 4 also includes A^U calculated by

$$A^{\mathrm{U}}=5\frac{G_{\mathrm{V}}}{G_{\mathrm{R}}}+\frac{B_{\mathrm{V}}}{B_{\mathrm{R}}}-6. \tag{6}$$

It can be seen that $Li_{13}Si_4$ has the smallest A^U value (0.11); the largest A^U value (1.30) is for $Li_{22}Si_5$. Thus, $Li_{22}Si_5$ has the strongest elastic anisotropy, which is consistent with the above analysis.

Table 4 Calculated shear anisotropic factors of the studied compounds

Alloy	A_1	A_2	A_3	A_z	A_B	A_G	A^U
LiSi	1.57	1.61	0.90	–	0%	2%	0.25
$Li_{12}Si_7$	0.72	0.71	0.58	–	3%	1%	0.20
$Li_{13}Si_4$	0.69	0.63	0.87	–	0%	1%	0.11
$Li_{15}Si_4$	–	–	–	2.28	0%	8%	0.86
$Li_{17}Si_4$	–	–	–	1.68	0%	3%	0.33
$Li_{22}Si_5$	–	–	–	2.71	0%	11%	1.30

3.4 Anisotropy of acoustic velocity

It is important to investigate the acoustic velocity, and we used the procedure of Brugger (Anderson, 1963), in longitudinal and transverse modes along the principal directions.

For a cubic system, there are three phonon independent propagation directions: [100], [110], and [111], and their corresponding sound velocities of both longitudinal and transverse waves along three different crystal directions are as follows:

$$[100]v_{\mathrm{l}}=\sqrt{\frac{C_{11}}{\rho}},\quad [010]v_{\mathrm{t1}}=[001]v_{\mathrm{t2}}=\sqrt{\frac{C_{44}}{\rho}},$$
$$[110]v_{\mathrm{l}}=\sqrt{\frac{C_{11}+C_{12}+2C_{44}}{2\rho}},\quad [1\bar{1}0]v_{\mathrm{t1}}=\sqrt{\frac{C_{11}-C_{12}}{\rho}},$$
$$[001]v_{\mathrm{t2}}=\sqrt{\frac{C_{44}}{\rho}},\quad [111]v_{\mathrm{l}}=\sqrt{\frac{C_{11}+2C_{12}+4C_{44}}{3\rho}},$$
$$[11\bar{2}]v_{\mathrm{t1}}=v_{\mathrm{t2}}=\sqrt{\frac{C_{11}-C_{12}+C_{44}}{3\rho}}. \tag{7}$$

For an orthorhombic system, the independent phonon propagation directions are [100], [010], and [001], and the corresponding sound velocities are

$$[100]v_{\mathrm{l}}=\sqrt{\frac{C_{11}}{\rho}},\quad [010]v_{\mathrm{t1}}=\sqrt{\frac{C_{66}}{\rho}},\quad [001]v_{\mathrm{t2}}=\sqrt{\frac{C_{55}}{\rho}},$$
$$[010]v_{\mathrm{l}}=\sqrt{\frac{C_{22}}{\rho}},\quad [100]v_{\mathrm{t1}}=\sqrt{\frac{C_{66}}{\rho}},\quad [001]v_{\mathrm{t2}}=\sqrt{\frac{C_{44}}{\rho}},$$
$$[001]v_{\mathrm{l}}=\sqrt{\frac{C_{33}}{\rho}},\quad [100]v_{\mathrm{t1}}=\sqrt{\frac{C_{55}}{\rho}},\quad [010]v_{\mathrm{t2}}=\sqrt{\frac{C_{44}}{\rho}}. \tag{8}$$

For a tetragonal system, the independent phonon propagation directions are [010], [001], and [110], and the corresponding sound velocities are

$$[010]v_{\mathrm{l}}=\sqrt{\frac{C_{11}}{\rho}},\quad [001]v_{\mathrm{t1}}=\sqrt{\frac{C_{44}}{\rho}},\quad [010]v_{\mathrm{t2}}=\sqrt{\frac{C_{66}}{\rho}},$$
$$[001]v_{\mathrm{l}}=\sqrt{\frac{C_{33}}{\rho}},\quad [100]v_{\mathrm{t1}}=[010]v_{\mathrm{t2}}=\sqrt{\frac{C_{66}}{\rho}},$$
$$[110]v_{\mathrm{l}}=\sqrt{\frac{(C_{11}+C_{12}+2C_{66})}{2\rho}},\quad [001]v_{\mathrm{t1}}=\sqrt{\frac{C_{44}}{\rho}},$$
$$[1\bar{1}0]v_{\mathrm{t2}}=\sqrt{\frac{(C_{11}-C_{12})}{2\rho}}, \tag{9}$$

where ρ is the density, v_l is the longitudinal sound velocity, and v_{t1} and v_{t2} represent the first and the second transverse modes, respectively.

Table 5 lists the sound velocities in different directions for the studied Li-Si alloys. The longitudinal acoustic velocities ([100]v_l, [001]v_l, [110]v_l, [111]v_l, and [010]v_l) are greater than the corresponding transverse modes. The longitudinal wave for a cubic system is the fastest along the [111] direction, while it is the fastest along the [001] direction for an orthorhombic system and along the [010] direction for a tetragonal system.

The Debye temperature (Θ_D) can determine the thermal properties of compounds. It can be calculated by the equation in (Pitzer, 1939). v_m is the mean sound velocity and is given by

$$v_m=\left[\frac{1}{3}\left(\frac{2}{v_t^3}+\frac{1}{v_l^3}\right)\right]^{-1/3}, \quad (10)$$

where v_t and v_l, the transverse and longitudinal sound velocities, are calculated by the following equations (Cahill et al., 1992):

$$v_t=\left(\frac{G}{\rho}\right)^{1/2}, \quad v_l=\left[\frac{B+(4G/3)}{\rho}\right]^{1/2}. \quad (11)$$

The calculated Θ_D, v_t, and v_l are included in Table 5. Θ_D increases in the sequence $Li_{15}Si_4$<LiSi< $Li_{22}Si_5$<$Li_{12}Si_7$<$Li_{13}Si_4$<$Li_{17}Si_4$. The higher Θ_D (691.02 K) for $Li_{17}Si_4$ implies its higher hardness, which is in line with the obtained hardness in Table 2. No experimental data are available but our investigation can estimate the mechanical properties of the studied Li-Si alloys.

3.5 Thermal conductivity

Thermal conductivity is closely related to the physical properties of materials under high temperature (Clarke, 2003). It comprises the lattice and electronic thermal conductivity. The total thermal conductivities of materials are mainly due to the lattice thermal conductivities because of the limitation of electronic thermal conductivity under low temperatures. The Cahill model (Cahill et al., 1992) and Clark model (Clarke, 2003) were used to calculate the minimum thermal conductivity.

$$\text{Cahill model: } K_{min}=\frac{k_B}{2.48}n^{2/3}(v_l+v_{t1}+v_{t2}), \quad (12)$$

$$\text{Clark model: } K_{min}=0.87k_BM_a^{-2/3}E^{1/2}\rho^{1/6}, \quad (13)$$

where k_B is Boltzmann constant, M_a is the mean atomic mass in a lattice and $M_a=M/(mN_A)$, M is the molar mass, m and n are the number of atoms in a

Table 5 Anisotropic sound velocity, mean sound velocity, density, and the Debye temperature for the Li-Si alloys

Parameter		Value					
		LiSi	$Li_{12}Si_7$	$Li_{13}Si_4$	$Li_{15}Si_4$	$Li_{17}Si_4$	$Li_{22}Si_5$
[100]	[100]v_l (km/s)	–	7.80	8.28	6.49	7.10	6.43
	[010]v_{t1} (km/s)	–	4.16	5.10	5.22	5.62	5.60
	[001]v_{t2} (km/s)	–	4.60	4.52	5.22	5.62	5.60
	[010]v_l (km/s)	7.53	–	–	–	–	–
	[001]v_{t1} (km/s)	4.91	–	–	–	–	–
	[010]v_{t2} (km/s)	4.51	–	–	–	–	–
[110]	[110]v_l (km/s)	7.39	–	–	7.58	7.95	7.82
	[1 $\bar{1}$ 0]v_{t1} (km/s)	–	–	–	4.90	6.13	4.81
	[001]v_{t2} (km/s)	–	–	–	5.22	5.62	5.60
	[001]v_{t1} (km/s)	4.91	–	–	–	–	–
	[1 $\bar{1}$ 0]v_{t2} (km/s)	4.74	–	–	–	–	–
[111]	[111]v_l (km/s)	–	–	–	7.91	8.21	8.23
	[11$\bar{2}$]v_{t1}, v_{t2} (km/s)	–	–	–	4.13	4.80	4.26
[010]	[010]v_l (km/s)	–	8.09	8.28	–	–	–
	[100]v_{t1} (km/s)	–	4.16	5.10	–	–	–
	[001]v_{t2} (km/s)	–	4.53	4.70	–	–	–
[001]	[001]v_l (km/s)	6.66	8.13	8.28	–	–	–
	[100]v_{t1} (km/s)	4.51	4.60	4.52	–	–	–
	[010]v_{t2} (km/s)	4.51	4.53	4.70	–	–	–
v_l (km/s)		7.47	7.43	7.82	7.23	7.71	7.35
v_t (km/s)		4.51	4.82	5.10	4.43	5.06	4.59
v_m (km/s)		4.99	5.29	5.59	4.89	5.55	5.05
Density, ρ (g/cm^3)		1.87	1.56	1.27	1.21	1.33	1.21
Debye temperature, Θ_D (K)		595.57	629.75	667.12	582.69	691.02	612.23

molecule and a unit volume, respectively, and N_A is Avogadro's number.

The minimum thermal conductivity for a Cahill model can determine its anisotropy. Table 6 lists the minimum thermal conductivities K_{min} of the studied Li-Si alloys. K_{min} obtained by the Clark model are less than those obtained by the Cahill model except for $Li_{22}Si_5$. All studied Li-Si alloys have low thermal conductivities and are thus not promising as thermal conductors. For tetragonal LiSi, [001]K_{min} is smaller than [100]K_{min} and [110]K_{min}. For orthorhombic $Li_{12}Si_7$ and $Li_{13}Si_4$, thermal conductivities along the three different directions are comparable, which indicates their isotropic properties. For cubic $Li_{15}Si_4$, $Li_{17}Si_4$, and $Li_{22}Si_5$, [110]K_{min} is greater than [100]K_{min} and [111]K_{min}, indicating their anisotropic properties.

3.6 Optical properties

The optical properties of crystals are important in industrial applications. We investigated the optical properties of Li-Si alloys, such as dielectric function. For the dielectric function $\varepsilon(\omega)=\varepsilon_1(\omega)+i\varepsilon_2(\omega)$, the real part $\varepsilon_1(\omega)$ is related to the electronic polarizability of the material (Debye, 1912). The peak of the imaginary part $\varepsilon_2(\omega)$ relates to the electron excitation.

Fig. 3 presents the dielectric functions of the studied Li-Si alloys as a function of photon energy from 0 to 20 eV. There are two spectral regions for the studied Li-Si alloys. The low energy ranges from 0 to 20 eV and the high energy ranges from 45 to 55 eV. From Fig. 3, the studied Li-Si alloys exhibit anisotropic behavior in the lower energy range. $\varepsilon_1(\omega)$ decreases sharply with the increase of photon energy and goes through zero in the low energy range, which indicates the metallic character of the studied Li-Si alloys. The static dielectric constants $\varepsilon_1(0)$ are 37.3, 49.4, 33.7, 47.5, 164.7, and 219.7 eV for LiSi, $Li_{12}Si_7$, $Li_{13}Si_4$, $Li_{15}Si_4$, $Li_{17}Si_4$, and $Li_{22}Si_5$, respectively. The larger static dielectric constants show that the studied Li-Si alloys are potential dielectric material (Rahman et al., 2016). Among the studied Li-Si alloys, $Li_{22}Si_5$ has the largest static dielectric constant, so it is an excellent dielectric material. The imaginary part $\varepsilon_2(\omega)$ firstly increases and then decreases with the increase of photon energy. The photon energies for the first dielectric peak of $\varepsilon_2(\omega)$ are 1.94, 0.77, 2.07, 0.97, 0.27, and 0.15 eV for LiSi, $Li_{12}Si_7$, $Li_{13}Si_4$, $Li_{15}Si_4$, $Li_{17}Si_4$, and $Li_{22}Si_5$, respectively, and are caused by the charge transfer between Li and Si atoms. A material is transparent when $\varepsilon_2(\omega)$ equals zero. When $\varepsilon_2(\omega)$ is not equal to zero, absorption begins. The values of $\varepsilon_2(\omega)$ become zero at about 16.8, 15.3, 13.8, 13.4, 14.1, and 13.5 eV for LiSi, $Li_{12}Si_7$, $Li_{13}Si_4$, $Li_{15}Si_4$, $Li_{17}Si_4$, and $Li_{22}Si_5$, respectively, which means the studied Li-Si alloys are transparent above 17 eV. The nonzero value of $\varepsilon_2(\omega)$ indicates the start of the absorption.

Fig. 4 presents the reflectivity $R(\omega)$, absorption coefficient $\alpha(\omega)$, and electron energy loss function $L(\omega)$ of the Li-Si alloys as a function of photon energy. From Fig. 4a, the studied Li-Si alloys have higher reflectivity from 0 to 20 eV. This shows that these materials are good coating materials in the ultraviolet region. In addition, we also notice a reflectivity peak

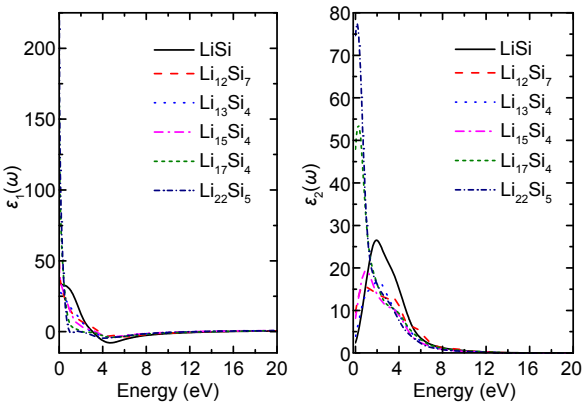

Fig. 3 Dielectric functions of the studied Li-Si alloys

Table 6 Mean atomic mass, number of atoms of unit volume, and minimum thermal conductivity for Li-Si alloys

Alloy	M_a ($\times10^{-23}$ g)	K_{min} (Clark) (W/(m·K))	n ($\times10^{28}$)	K_{min} (Cahill) (W/(m·K))	[100]K_{min} (W/(m·K))	[110]K_{min} (W/(m·K))	[111]K_{min} (W/(m·K))	[010]K_{min} (W/(m·K))	[001]K_{min} (W/(m·K))
LiSi	2.91	0.91	3.2	0.93	2.36	2.38	–	–	2.19
$Li_{12}Si_7$	2.45	0.92	3.4	0.99	0.51	–	–	0.52	0.53
$Li_{13}Si_4$	1.98	0.96	3.8	1.13	0.60	–	–	0.60	0.59
$Li_{15}Si_4$	1.90	0.82	3.4	0.93	0.52	0.55	0.50	–	–
$Li_{17}Si_4$	1.83	1.04	3.5	1.05	0.58	0.62	0.56	–	–
$Li_{22}Si_5$	1.80	0.87	2.5	0.78	0.45	0.46	0.42	–	–

around 56 eV. From Fig. 4b, the absorption coefficients form two peaks, one is wider at the lower energies, and the other is narrower at 56 eV. Fig. 4c shows that the energy loss spectra of all the studied Li-Si alloys have two peaks; one is sharp when the energy is low, and the other is gentler at the higher energy. The first sharp peak is associated with plasma oscillation and corresponds to the bulk plasma frequency ω_p. The maximum peaks for LiSi, $Li_{12}Si_7$, $Li_{13}Si_4$, $Li_{15}Si_4$, $Li_{17}Si_4$, and $Li_{22}Si_5$ are at the photon energies of 14.8, 13.7, 12.7, 12.4, 13.7, and 12.7 eV, respectively.

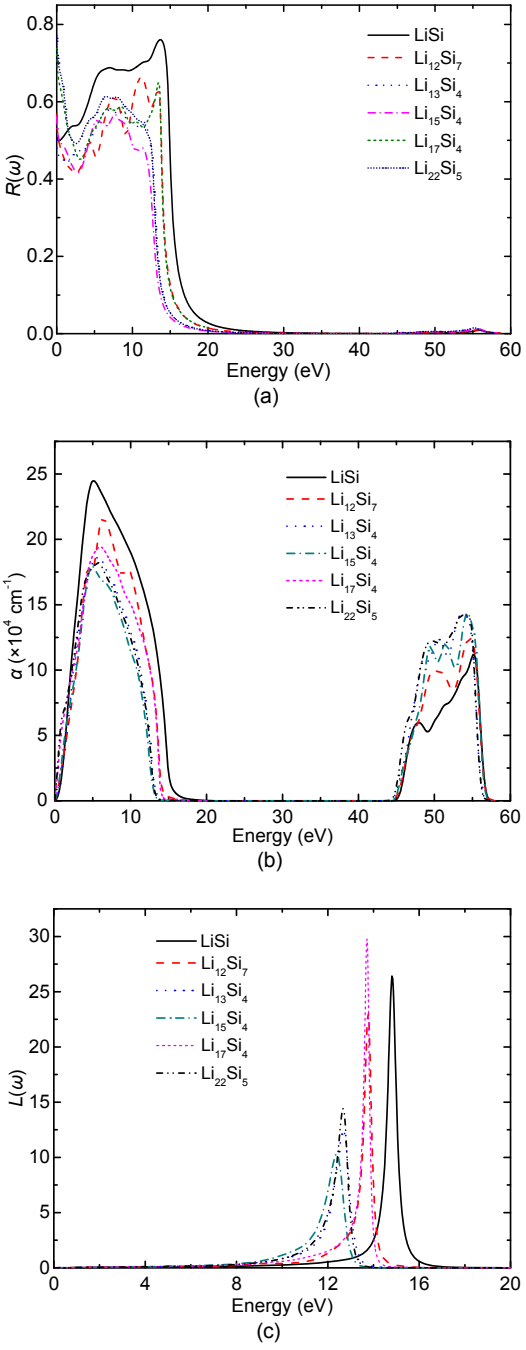

Fig. 4 Optical properties of the studied Li-Si alloys: (a) reflectivity; (b) absorption coefficient; (c) electron energy loss function

4 Conclusions

We have investigated the elastic, acoustic, and optical properties of several Li-Si alloys by density functional calculations. Results show these Li-Si alloys are mechanically stable and brittle, and have a covalent character. Their bulk moduli increase with increasing lithium content, so they are more difficult to compress as the lithium content increases. All the studied Li-Si alloys have a significant anisotropic Young's modulus and exhibit the butterfly-shaped curves on some planes. The sequence of degree of anisotropic Young's modulus is $Li_{22}Si_5$>$Li_{15}Si_4$>LiSi>$Li_{17}Si_4$>$Li_{12}Si_7$>$Li_{13}Si_4$. The anisotropy of acoustic velocity was also investigated. The longitudinal wave along the [111] direction is the fastest for the cubic system, while it is the fastest along the [001] direction for the orthorhombic system and along the [010] direction for the tetragonal system. The higher Debye temperature (691.02 K) for $Li_{17}Si_4$ implies it is harder than the other studied Li-Si alloys. All the studied Li-Si alloys have relatively low thermal conductivities and are promising dielectric materials.

Contributors

Xiao-hong LI designed the research and wrote the first draft and final version of the manuscript. Hong-ling CUI processed the corresponding data. Rui-zhou ZHANG helped to revise the manuscript.

Conflict of interest

Xiao-hong LI, Hong-ling CUI, and Rui-zhou ZHANG declare that they have no conflict of interest.

References

Anderson OL, 1963. A simplified method for calculating the Debye temperature from elastic constants. *Journal of Physics and Chemistry of Solids*, 24(7):909-917. https://doi.org/10.1016/0022-3697(63)90067-2

Born M, 1940. On the stability of crystal lattices. I. *Mathematical Proceedings of the Cambridge Philosophical Society*, 36(2):160-172.

https://doi.org/10.1017/S0305004100017138

Braga MH, Dębski A, Gąsior W, 2014. Li-Si phase diagram: enthalpy of mixing, thermodynamic stability, and coherent assessment. *Journal of Alloys and Compounds*, 616: 581-593.
https://doi.org/10.1016/j.jallcom.2014.06.212

Cahill DG, Watson SK, Pohl RO, 1992. Lower limit to the thermal conductivity of disordered crystals. *Physical Review B*, 46(10):6131-6140.
https://doi.org/10.1103/PhysRevB.46.6131

Chen XQ, Niu HY, Li DZ, et al., 2011. Modeling hardness of polycrystalline materials and bulk metallic glasses. *Intermetallics*, 19(9):1275-1281.
https://doi.org/10.1016/j.intermet.2011.03.026

Chen XW, Yu XB, 2012. Electronic structure and initial dehydrogenation mechanism of $M(BH_4)_2{\cdot}2NH_3$ (M=Mg, Ca, and Zn): a first-principles investigation. *The Journal of Physical Chemistry C*, 116(22):11900-11906.
https://doi.org/10.1021/jp301986k

Cheng YT, Verbrugge MW, 2010. Application of Hasselman's crack propagation model to insertion electrodes. *Electrochemical and Solid-State Letters*, 13(9):A128-A131.
https://doi.org/10.1149/1.3455179

Chevrier VL, Zwanziger JW, Dahn JR, 2009. First principles studies of silicon as a negative electrode material for lithium-ion batteries. *Canadian Journal of Physics*, 87(6): 625-632.
https://doi.org/10.1139/P09-031

Chevrier VL, Zwanziger JW, Dahn JR, 2010. First principles study of Li-Si crystalline phases: charge transfer, electronic structure, and lattice vibrations. *Journal of Alloys and Compounds*, 496(1-2):25-36.
https://doi.org/10.1016/j.jallcom.2010.01.142

Clarke DR, 2003. Materials selection guidelines for low thermal conductivity thermal barrier coatings. *Surface and Coatings Technology*, 163-164:67-74.
https://doi.org/10.1016/S0257-8972(02)00593-5

Cui ZW, Gao F, Cui ZH, et al., 2012. A second nearest-neighbor embedded atom method interatomic potential for Li–Si alloys. *Journal of Power Sources*, 207:150-159.
https://doi.org/10.1016/j.jpowsour.2012.01.145

Debye P, 1912. Zur Theorie der spezifischen Wärmen. *Annalen Der Physik*, 344(14):789-839 (in German).
https://doi.org/10.1002/andp.19123441404

Furthmüller J, Käckell P, Bechstedt F, et al., 2000. Extreme softening of Vanderbilt pseudopotentials: general rules and case studies of first-row and d-electron elements. *Physical Review B*, 61(7):4576-4587.
https://doi.org/10.1103/PhysRevB.61.4576

Guechi N, Bouhemadou A, Khenata R, et al., 2014. Structural, elastic, electronic and optical properties of the newly synthesized monoclinic Zintl phase $BaIn_2P_2$. *Solid State Science*, 29:12-23.
https://doi.org/10.1016/j.solidstatesciences.2014.01.001

Hill R, 1952. The elastic behaviour of a crystalline aggregate. *Proceedings of the Physical Society. Section A*, 65(5): 349-354.
https://doi.org/10.1088/0370-1298/65/5/307

Key B, Bhattacharyya R, Morcrette M, et al., 2009. Real-time NMR investigations of structural changes in silicon electrodes for lithium-ion batteries. *Journal of the American Chemical Society*, 131(26):9239-9249.
https://doi.org/10.1021/ja8086278

Kim H, Chou CY, Ekerdt JG, et al., 2011. Structure and properties of Li−Si alloys: a first-principles study. *The Journal of Physical Chemistry C*, 115(5):2514-2521.
https://doi.org/10.1021/jp1083899

McDowell MT, Lee SW, Harris JT, et al., 2013. In situ TEM of two-phase lithiation of amorphous silicon nanospheres. *Nano Letters*, 13(2):758-764.
https://doi.org/doi/abs/10.1021/nl3044508

Miao NH, Sa BS, Zhou J, et al., 2011. Theoretical investigation on the transition-metal borides with Ta_3B_4-type structure: a class of hard and refractory materials. *Computational Materials Science*, 50(4):1559-1566.
https://doi.org/10.1016/j.commatsci.2010.12.015

Min SH, Jo MR, Song DH, et al., 2016. High crystalline carbon network of Si/C nanofibers obtained from the embedded pitch and its contribution to Li ion kinetics. *Electrochimica Acta*, 220:511-516.
https://doi.org/10.1016/j.electacta.2016.10.111

Mott NF, Jones H, 1958. The Theory of the Properties of Metals and Alloys. Dover Publications, New York, USA, p.65-68.

Mouhat F, Coudert FX, 2014. Necessary and sufficient elastic stability conditions in various crystal systems. *Physical Review B*, 90(22):224104.
https://doi.org/10.1103/PhysRevB.90.224104

Newnham RE, 2005. Properties of Materials: Anisotropy, Symmetry, Structure. Oxford University Press, New York, USA, p.210-214.

Nye FJ, 1985. Physical Properties of Crystals. Oxford University Press, Oxford, UK, p.153-155.

Obrovac MN, Christensen L, 2004. Structural changes in silicon anodes during lithium insertion/extraction. *Electrochemical and Solid-State Letters*, 7(5):A93-A96.
https://doi.org/10.1149/1.1652421

Perdew JP, Burke K, Ernzerhof M, 1996. Generalized gradient approximation made simple. *Physical Review Letters*, 77(18):3865-3868.
https://doi.org/10.1103/PhysRevLett.77.3865

Pfrommer BG, Côté M, Louie SG, et al., 1997. Relaxation of crystals with the quasi-Newton method. *Journal of Computational Physics*, 131(1):233-240.
https://doi.org/10.1006/jcph.1996.5612

Pitzer KS, 1939. Corresponding states for perfect liquids. *The*

Journal of Chemical Physics, 7(8):583-590. https://doi.org/10.1063/1.1750496

Pugh SF, 1954. XCII. Relations between the elastic moduli and the plastic properties of polycrystalline pure metals. *The London, Edinburgh, and Dublin Philosophical Magazine and Journal of Science*, 45(367):823-843. https://doi.org/10.1080/14786440808520496

Rahman MA, Rahaman MZ, Rahman MA, 2016. The structural, elastic, electronic and optical properties of MgCu under pressure: a first-principles study. *International Journal of Modern Physics B*, 30(27):1650199. https://doi.org/10.1142/S021797921650199X

Ranganathan SI, Ostoja-Starzewski M, 2008. Universal elastic anisotropy index. *Physical Review Letters*, 101(5): 055504-4. https://doi.org/10.1103/PhysRevLett.101.055504

Ratchford JB, Schuster BE, Crawford BA, et al., 2011. Young's modulus of polycrystalline $Li_{22}Si_5$. *Journal of Power Sources*, 196(18):7747-7749. https://doi.org/10.1016/j.jpowsour.2011.04.042

Ratchford JB, Crawford BA, Wolfenstine J, et al., 2012. Young's modulus of polycrystalline $Li_{12}Si_7$ using nanoindentation testing. *Journal of Power Sources*, 211: 1-3. https://doi.org/10.1016/j.jpowsour.2012.02.027

Ravindran P, Fast L, Korzhavyi PA, et al., 1998. Density functional theory for calculation of elastic properties of orthorhombic crystals: application to $TiSi_2$. *Journal of Applied Physics*, 84(9):4891-4901. https://doi.org/10.1063/1.368733

Reuss A, 1929. Berechnung der fließgrenze von mischkristallen auf grund der plastizitätsbedingung für einkristalle. *Zeitschrift für Angewandte Mathematik und Mechanik*, 9(1):49-58 (in German). https://doi.org/10.1002/zamm.19290090104

Savin A, Flad HJ, Flad J, et al., 1992. On the bonding in carbosilanes. *Angewandte Chemie International Edition*, 31(2):185-187. https://doi.org/10.1002/anie.199201851

Schwalbe S, Gruber T, Trepte K, et al., 2017. Mechanical, elastic and thermodynamic properties of crystalline lithium silicides. *Computational Materials Science*, 134:48-57. https://doi.org/10.1016/j.commatsci.2017.03.028

Shenoy VB, Johari P, Qi Y, 2010. Elastic softening of amorphous and crystalline Li-Si phases with increasing Li concentration: a first-principles study. *Journal of Power Sources*, 195(19):6825-6830. https://doi.org/10.1016/j.jpowsour.2010.04.044

Sin'ko GV, Smirnov NA, 2002. *Ab initio* calculations of elastic constants and thermodynamic properties of bcc, fcc, and hcp Al crystals under pressure. *Journal of Physics: Condensed Matter*, 14(29):6989-7005. https://doi.org/10.1088/0953-8984/14/29/301

Su X, Wu QL, Li JC, et al., 2014. Silicon-based nanomaterials for lithium-ion batteries: a review. *Advanced Energy Materials*, 4(1):1300882. https://doi.org/10.1002/aenm.201300882

Sun L, Gao YM, Xiao B, et al., 2013. Anisotropic elastic and thermal properties of titanium borides by first-principles calculations. *Journal of Alloys and Compounds*, 579:457-467. https://doi.org/10.1016/j.jallcom.2013.06.119

Sun L, Su TT, Xu L, et al., 2016. Preparation of uniform Si nanoparticles for high-performance Li-ion battery anodes. *Physical Chemistry Chemical Physics*, 18(3):1521-1525. https://doi.org/10.1039/C5CP06585B

Tipton WW, Bealing CR, Mathew K, et al., 2013. Structures, phase stabilities, and electrical potentials of Li–Si battery anode materials. *Physical Review B*, 87(18):184114. https://doi.org/10.1103/PhysRevB.87.184114

Voigt W, 1928. Lehrbuch der Kristallphysik: Teubner-Leipzig. Macmillan, New York, USA, p.112-115.

Wang YX, Liu B, Li QY, et al., 2015. Lithium and lithium ion batteries for applications in microelectronic devices: a review. *Journal of Power Sources*, 286:330-345. https://doi.org/10.1016/j.jpowsour.2015.03.164

Wu H, Zheng GY, Liu N, et al., 2012. Engineering empty space between Si nanoparticles for lithium-ion battery anodes. *Nano Letters*, 12(2):904-909. https://doi.org/10.1021/nl203967r

Xu K, von Cresce A, 2011. Interfacing electrolytes with electrodes in Li ion batteries. *Journal of Materials Chemistry*, 21(27):9849-9864. https://doi.org/10.1039/c0jm04309e

Zeilinger M, Benson D, Häussermann U, et al., 2013. Single crystal growth and thermodynamic stability of $Li_{17}Si_4$. *Chemistry of Materials*, 25(9):1960-1967. https://doi.org/10.1021/cm400612k

Zeng MX, Wang RN, Tang BY, et al., 2012. Elastic and electronic properties of tI26-type $Mg_{12}RE$ (RE=Ce, Pr and Nd) phases. *Modelling and Simulation in Materials Science and Engineering*, 20(3):035018. https://doi.org/10.1088/0965-0393/20/3/035018

Zeng ZD, Liu N, Zeng QS, et al., 2013. Elastic moduli of polycrystalline $Li_{15}Si_4$ produced in lithium ion batteries. *Journal of Power Sources*, 242:732-735. https://doi.org/10.1016/j.jpowsour.2013.05.121

Zhang SC, Du ZJ, Lin RX, et al., 2010. Nickel nanocone-array supported silicon anode for high-performance lithium-ion batteries. *Advanced Materials*, 22(47):5378-5382. https://doi.org/10.1002/adma.201003017

Zhang WJ, 2011. A review of the electrochemical performance of alloy anodes for lithium-ion batteries. *Journal of Power Sources*, 196(1):13-24. https://doi.org/doi.org/10.1016/j.jpowsour.2010.07.020

Zhao KJ, Wang WL, Gregoire J, et al., 2011. Lithium-assisted plastic deformation of silicon electrodes in lithium-ion batteries: a first-principles theoretical study. *Nano Letters*, 11(7):2962-2967. https://doi.org/10.1021/nl201501s

Zhao XY, Wang JL, Luo H, et al., 2016. A novel organosilicon-based ionic plastic crystal as solid-state electrolyte for lithium-ion batteries. *Journal of Zhejiang University-SCIENCE A (Applied Physics & Engineering)*, 17(2):155-162. https://doi.org/10.1631/jzus.A1500099

Zheng JM, Engelhard MH, Mei DH, et al., 2017. Electrolyte additive enabled fast charging and stable cycling lithium metal batteries. *Nature Energy*, 2(3):17012. https://doi.org/10.1038/nenergy.2017.12

List of electronic supplementary materials

Fig. S1 Crystal structures of the Li-Si alloys.
Data S1 Equations.
Fig. S2 Directional bulk modulus and Young's modulus of the studied materials on other atomic planes.
Table S1 Elastic compliance constants of the studied Li-Si alloys.

中文概要

题　目：锂硅合金的力学、声学及光学性质的第一性原理研究

概　要：锂硅合金作为潜在的锂离子电池已被广泛研究。了解锂硅合金的力学、声学和光学性质对于改进电池的性能非常重要。本文从理论上研究了几种锂硅合金的一系列特性。研究表明，这些锂硅合金具有力学稳定性。随着锂浓度的增加，锂硅合金中 Si-Si 键减少，从而使其越来越容易变形。弹性模量的分析表明，随着锂浓度的增加，体模量增加，且 $Li_{22}Si_5$ 的杨氏模量各向异性最强。杨氏模量各向异性强度的次序为：$Li_{22}Si_5$>$Li_{15}Si_4$>LiSi>$Li_{17}Si_4$>$Li_{12}Si_7$>$Li_{13}Si_4$。从声速的各向异性分析得知，横向声速小于相应的纵向声速。立方体系的纵波在[111]方向最快，正交体系的纵波在[001]方向最快，而四方晶系的纵波在[010]方向最快。所研究的锂硅合金的导热性较低，且当光子能量小于 20 eV 时，显示出较高的各向异性。

关键词：力学特性；导热性；锂离子电池；弹性各向异性；第一性原理计算